RSC Advances

PAPER

View Article Online
View Journal | View Issue

Cite this: *RSC Adv.*, 2016, **6**, 98071

Enhancing the photovoltaic performance of binary acceptor-based conjugated polymers incorporating methyl units†

Guitao Feng,[ab] Yunhua Xu,*[a] Yang Wu,[c] Cheng Li,[b] Fan Yang,[b] Yaping Yu,[b] Wei Ma*[c] and Weiwei Li*[b]

Received 14th July 2016
Accepted 10th October 2016

DOI: 10.1039/c6ra17986j

www.rsc.org/advances

Three conjugated polymers incorporating pentacyclic lactam (PCL) and diketopyrrolopyrrole (DPP) units into conjugated polymers were designed and synthesized, in which the aromatic linkers between PCL and DPP varied from thiophene to methylthiophene. Methylated polymers were found to show slightly blue-shift absorption and high-lying energy levels compared to non-methylated polymers. The three polymers also exhibit good crystalline properties and hole mobilities up to 0.57 $cm^2 V^{-1} s^{-1}$ in field-effect transistors. Non-methylated polymers as electron donors in solar cells show an efficiency of 4.2% with a relatively low short circuit current density (J_{sc}) of 8.3 mA cm^{-2}, while methylated polymers exhibit dramastically enhanced J_{sc} of 12.8 mA cm^{-2} and PCEs up to 6.1%. Micro-phase separation in bulk-heterojunction thin films were systematically investigated, in which methylated polymers in blended thin films were found to provide better micro-phase separation with small crystal domain. The observation can explain their improved photocurrent in solar cells. Our studies demonstrate that by intentionally structural modification, conjugated polymers containing several electron-deficient units can have the great potential application in high performance solar cells.

Introduction

Polymer solar cells (PSCs) have made great progress in the last two decades with power conversion efficiencies (PCEs) approach 12%,[1,2] demonstrating their potential application in large-area and flexible devices.[3] The high performance is partially attributed to the materials development of conjugated polymers, such as constructing from electron-donating and electron-withdrawing units, as so called "donor–acceptor" polymers.[4,5] In order to further enhance the performance, new conjugated polymers are required to be developed, concerning their absorption spectra, energy levels, crystalline properties and charge carrier mobilities. In particular, conjugated polymers with deep lowest unoccupied molecular orbital (LUMO) levels are very useful since they can provide low LUMO offset when combining with fullerene derivatives, such as [6,6]-phenyl-C71-butyric acid methyl ester ([70]PCBM) as electron acceptor. This will lower the energy loss (E_{loss})[6] between optical band gap (E_g) and open circuit voltage (V_{oc}) and further enhance the PCEs of solar cells.[7–12]

The designation by incorporating binary electron-deficient units into conjugated polymers is an efficient route to realize deep LUMO levels.[13–21] In general, introducing strong electron-donating moieties into conjugated polymers is helpful for realizing high-lying highest occupied molecular orbital (HOMO) levels, while strong electron-deficient units can reduce the LUMO levels of conjugated polymers. When introducing two electron-deficient units into conjugated backbone, deep LUMO levels can be easily realized. In our previous work, we design a conjugated polymer using a weak electron-deficient pentacyclic lactam (PCL) unit and a strong electron-deficient diketopyrrolopyrrole (DPP) unit.[13] The polymer showed a low LUMO level of −3.89 eV and good crystalline property. Solar cells based on this polymer as donor exhibit a PCE of 4.7% with a small E_{loss} of 0.65 eV. Since we found that the polymer showed near-infrared absorption up to 900 nm and a high mobility of 0.81 $cm^2 V^{-1} s^{-1}$, we speculate that this polymer has the potential to realize better PCEs if finely tuned chemical structures can be provided.

With this purpose, we are dedicated to exploring new conjugated polymers based on PCL and DPP units in order to improve the PCEs in solar cells. DPP-based compounds contain aromatic linkers due to the synthetic nature of DPP units.[22] In our previous work,[13] the polymer was constructed by using thiophene (T) as linker, which is also widely reported in DPP

[a]*Department of Chemistry, School of Science, Beijing Jiaotong University, Beijing 100044, P. R. China. E-mail: yhxu@bjtu.edu.cn*

[b]*Beijing National Laboratory for Molecular Sciences, CAS Key Laboratory of Organic Solids, Institute of Chemistry, Chinese Academy of Sciences, Beijing 100190, P. R. China. E-mail: liweiwei@iccas.ac.cn*

[c]*State Key Laboratory for Mechanical Behavior of Materials, Xi'an Jiaotong University, Xi'an 710049, P. R. China. E-mail: msewma@xjtu.edu.cn*

† Electronic supplementary information (ESI) available. See DOI: 10.1039/c6ra17986j

polymers.[23,24] In this work, we intend to use methylthiophene (MT) to replace of T as linkers in the polymers. MT-based DPP polymers have been found to show slightly high-lying energy levels (both of HOMO and LUMO) but with similar absorption spectra as non-methylated DPP polymers.[25,26] This indicates that the energy offset between the polymer donor and PCBM as acceptor will increase. Since in bulk-heterojunction solar cells exciton is bounded by strong Coulomb force, so it requires excess energy to separate into free charges. Therefore, high energy offset will help the exciton separation and significantly increase the quantum efficiencies in solar cells. In this work, we explore two new conjugated polymers based PCL and DPP in the conjugated backbone, in which MT as linkers were introduced, as shown in Fig. 1. The new polymers were found to show slightly blue-shift absorption and high-lying energy levels compared to the polymer with T as linkers. In addition, the three polymers exhibit similar hole mobilities of 0.47–0.57 $cm^2 V^{-1} s^{-1}$ in field-effect transistors (FETs). The polymers were applied into solar cells, in which methylated polymers perform high PCEs up to 6.1% due to significantly enhanced short circuit current density (J_{sc}) of 12.8 mA cm^{-2}. As compare, non-methylated polymer with PCL and DPP units exhibits a J_{sc} of 8.3 mA cm^{-2} and PCE of 4.2%. Further investigation of morphology in blended thin films by atom force microscopy (AFM), transmission electron microscopy (TEM), grazing-incidence wide-angle X-ray scattering (GIWAXS) and resonant soft X-ray scattering (R-SoXS) reveals that methylated polymers in BHJ thin films show improved micro-phase separation with small crystal domain, explaining their high photocurrent in solar cells.

Experimental

Materials and measurements

All synthetic procedures were performed under argon atmosphere. Commercial chemicals (from Sigma-Aldrich, JK Chemical and TCI) were used as received. THF and toluene were distilled from sodium under an N_2 atmosphere. 4,10-Bis(2-hexyldecyl)thieno[2′,3′:5,6]pyrido[3,4-*g*]thieno[3,2-*c*]isoquinoline-5,11(4*H*,10*H*)-dione (**1**),[13] 3-(4-methylthiophen-2-yl)-6-(thiophen-2-yl)pyrrolo[3,4-*c*]pyrrole-1,4(2*H*,5*H*)-dione (**2**),[26] 3,6-bis(4-methylthiophen-2-yl)pyrrolo[3,4-*c*]pyrrole-1,4(2*H*,5*H*)-dione (**3**)[25] and 3,6-bis(5-bromothiophen-2-yl)-2,5-bis(2-ethylhexyl)pyrrolo[3,4-*c*]pyrrole-1,4(2*H*,5*H*)-dione (**M2**)[27] were synthesized according to literature procedures. ^{1}H-NMR and ^{13}C-NMR spectra were recorded at 400 MHz and 100 MHz on a Bruker AVANCE spectrometer with $CDCl_3$ as the solvent and tetramethylsilane (TMS) as the internal standard. Molecular weight was determined with GPC at 140 °C on a PL-GPC 220 system using a PL-GEL 10 μm MIXED-B column and *o*-DCB as the eluent against polystyrene standards. Low concentration of 0.1 mg mL^{-1} polymer in *o*-DCB was applied to reduce aggregation. Optical absorption spectra were recorded on a JASCO V-570 spectrometer with a slit width of 2.0 nm and a scan speed of 1000 nm min^{-1}. Cyclic voltammetry was performed under an inert atmosphere at a scan rate of 0.1 V s^{-1} and 1 M tetrabutylammonium hexafluorophosphate in acetonitrile as the electrolyte, a glassy-carbon working electrode coated with samples, a platinum-wire auxiliary electrode, and an Ag/AgCl as a reference electrode.

Atomic force microscopy (AFM) images were recorded using a Digital Instruments Nano scope IIIa multimode atomic force microscope in tapping mode under ambient conditions. Bright field TEM images were performed on a Hitachi SU8200 scanning electron microscope.

GIWAXS measurements were performed at beamline 7.3.3 (ref. 28) at the Advanced Light Source. Samples were prepared on Si substrates using identical blend solutions as those used in devices. The 10 keV X-ray beam was incident at a grazing angle of 0.12–0.16°, selected to maximize the scattering intensity from the samples. The scattered x-rays were detected using a Dectris Pilatus 2M photon counting detector.

R-SoXS transmission measurements were performed at beamline 11.0.1.2 (ref. 29) at the Advanced Light Source (ALS). Samples for R-SoXS measurements were prepared on a PEDOT:PSS modified Si substrate under the same conditions as those used for device fabrication, and then transferred by floating in water to a 1.5 mm × 1.5 mm, 100 nm thick Si_3N_4 membrane supported by a 5 mm × 5 mm, 200 μm thick Si frame (Norcada Inc.). 2-D scattering patterns were collected on an in-vacuum CCD camera (Princeton Instrument PI-MTE). The sample detector distance was calibrated from diffraction peaks of a triblock copolymer poly(isoprene-*b*-styrene-*b*-2-vinyl pyridine), which has a known spacing of 391 Å. The beam size at the sample is approximately 100 μm by 200 μm.

The organic field-effect transistors were fabricated on a commercial Si/SiO_2/Au substrate purchased from First MEMS Co. Ltd. A heavily N-doped Si wafer with a SiO_2 layer of 300 nm served as the gate electrode and dielectric layer, respectively. The Ti (2 nm)/Au (28 nm) source–drain electrodes were sputtered and patterned by a lift-off technique. Before deposition of the organic semiconductor, the gate dielectrics were treated with octadecyltrichlorosilane (OTS) in a vacuum oven at a temperature of 120 °C, forming an OTS self-assembled monolayers. The treated substrates were rinsed successively with hexane, chloroform, and isopropyl alcohol. Polymer thin films were spin coated on the substrate from solution with a thickness of around 30–50 nm. The devices were thermally annealed at the corresponding temperature in air for 10 min, cooled down and then moved into a glovebox

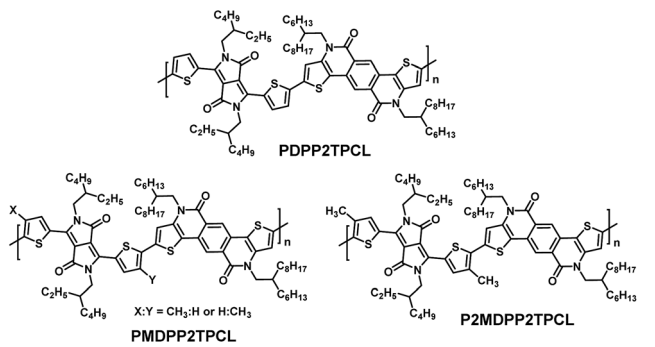

Fig. 1 The chemical structures of the polymers studied in this work.

filled with N_2. The devices were measured on an Keithley 4200 SCS semiconductor parameter analyzer at room temperature. The mobilities were calculated from the saturation region with the following equation: $I_{DS} = (W/2L)C_i\mu(V_G - V_T)^2$, where I_{SD} is the drain–source current, W is the channel width (1400 μm), L is the channel length (50 μm), μ is the field-effect mobility, C_i is the capacitance per unit area of the gate dielectric layer, and V_G and V_T are the gate voltage and threshold voltage, respectively. This equation defines the important characteristics of electron mobility (μ), on/off ratio (I_{on}/I_{off}), and threshold voltage (V_T), which could be deduced by the equation from the plot of current–voltage.

Photovoltaic devices were made by spin-coating poly-(ethylenedioxythiophene):poly(styrene sulfonate) (PEDOT:PSS) (Clevios P, VP AI 4083) onto pre-cleaned, patterned ITO substrates. The photoactive layers were deposited by spin coating a chloroform solution containing the DPP polymer, the electron acceptors and the appropriate amount of processing additive diphenylether (DPE) in air. LiF (1 nm) and Al (100 nm) were deposited by vacuum evaporation at *ca.* 4×10^{-5} Pa as the back electrode.

The active area of the cells was 0.04 cm^2. The *J*–*V* characteristics were measured by a Keithley 2400 source meter unit under AM1.5G spectrum from a solar simulator (Enlitech model SS-F5-3A). Solar simulator illumination intensity was determined at 100 mW cm^{-2} using a monocrystal silicon reference cell with KG5 filter. Short circuit currents under AM1.5G conditions were estimated from the spectral response and convolution with the solar spectrum. The external quantum efficiency was measured by a Solar Cell Spectral Response Measurement System QE-R3011 (Enli Technology Co., Ltd.). The thickness of the active layers in the photovoltaic devices was measured on a Veeco Dektak XT profilometer.

4,10-Bis(2-hexyldecyl)-2,8-bis(trimethylstannyl)-4,10-dihydrothieno[2′,3′:5,6]pyrido[3,4-*g*]thieno[3,2-*c*]isoquinoline-5,11-dione (M1). To a solution of compound **1** (225 mg, 0.29 mmol) in THF (10 mL) at −78 °C the freshly prepared LDA was added dropwise. The mixture was stirred at −78 °C for 2 hours and them 0.93 mL of trimethyltin chloride (1 M in hexanes) was added dropwise. After 2 hours, the mixture was poured into water (100 mL) and extracted with diethyl ether. The organic layer was washed with water and dried over magnesium sulphate. After drying solvent, the residue was purified by recrystallization from ethanol to give a yellow product **M1** (243 mg, 76%).^{1}H NMR δ (ppm): 8.88 (s, 2H), 7.16–7.04 (m, 2H), 4.25 (s, 4H), 2.04 (s, 2H), 1.30 (m, 48H), 0.84 (m, 12H), 0.59–0.35 (m, 18H). ^{13}C NMR δ (ppm): 161.94, 140.85, 140.37, 129.78, 126.46, 124.82, 124.11, 123.49, 49.64, 37.35, 32.03, 31.96, 31.92, 30.14, 29.81, 29.70, 29.43, 26.88, 22.80, 22.78, 14.22. MS (MALDI): calculated: 1098.85, found: 1098.4 (M^+).

3-(5-Bromo-4-methylthiophen-2-yl)-6-(5-bromothiophen-2-yl)-2,5-bis(2-ethylhexyl)pyrrolo[3,4-*c*]pyrrole-1,4(2*H*,5*H*)-dione (M3). To a solution of 2 (0.92 g, 2.93 mmol), potassium carbonate (1.52 g, 10.97 mmol), and 18-crown-6 (10 mg) in DMF (30 mL) was added 2-ethylhexyl bromide (1.70 g, 8.79 mmol). The reaction mixture was stirred at 120 °C for 16 h and then cooled to room temperature. $CHCl_3$ (100 mL) and water (100 mL) were added and the layers were separated. The organic layer was washed with brine and the solvent evaporated. The resulting solid was subjected to column chromatography (silica, eluent hexane/CH_2Cl_2, v/v 80/20) to afford 2,5-bis(2-ethylhexyl)-3-(4-methylthiophen-2-yl)-6-(thiophen-2-yl)pyrrolo[3,4-*c*]pyrrole-1,4(2*H*,5*H*)-dione as red solid (0.33 g, 20.9%).

To a solution of 2,5-bis(2-ethylhexyl)-3-(4-methylthiophen-2-yl)-6-(thiophen-2-yl)pyrrolo[3,4-*c*]pyrrole-1,4(2*H*,5*H*)-dione (0.33 g, 0.61 mmol), K_2CO_3 (0.50 g, 3.64 mmol) in $CHCl_3$ (20 mL) was added dropwise a Br_2 (1.86 g, 2.45 mmol) in $CHCl_3$(15 mL) solution in 10 min at 0 °C. The reaction mixture was stirred at room temperature for 10 min. Sodium thiosulfate (5 g, 20 mL H_2O) solution was added into reaction mixture and stirred for 30 min to remove Br_2. The mixture was washed with brine and the layers were separated. The resulting solid was subjected to column chromatography (silica, eluent hexane/CH_2Cl_2, v/v 80/20) to afford **M3** as crude product. The solid was dissolved in $CHCl_3$ (5 mL) and precipitated into methanol (100 mL) to afford pure **M3** (0.41 g, 99%) as a red solid.^{1}H NMR δ (ppm): 8.64–8.58 (m, 2H), 7.22 (d, 1H), 3.99–3.88 (m, 4H), 2.30 (s, 3H), 1.84 (s, 2H), 1.54 (s, 2H), 1.43–1.18 (m, 16H), 0.87 (m, 12H). ^{13}C NMR δ (ppm): 160.61, 138.94, 138.27, 135.83, 134.29, 130.51, 128.11, 117.90, 116.12, 107.34, 106.94, 76.42, 76.16, 75.84, 45.21, 38.29, 29.42, 27.55, 22.83, 22.18, 14.34, 13.13, 9.68. MS (MALDI): calculated: 696.60, found: 696.0 (M^+).

3,6-Bis(5-bromo-4-methylthiophen-2-yl)-2,5-bis(2-ethylhexyl)pyrrolo[3,4-*c*]pyrrole-1,4(2*H*,5*H*)-dione (M4). Same procedure as for **M3** was used, but now **3** (2 g, 8.4 mmol) was used as the reactant. Yield: 2.2 g (83.3%).^{1}H NMR δ (ppm): 8.57 (s, 2H), 3.93 (m, 4H), 2.30 (s, 4H), 1.84 (m, 2H), 1.53 (m, 4H), 1.46–1.09 (m, 12H), 0.87 (m, 9H). ^{13}C NMR δ (ppm): 160.65, 138.57, 138.30, 135.65, 128.18, 115.88, 107.06, 45.22, 38.30, 29.46, 27.59, 22.87, 22.20, 14.34, 13.14, 9.74. MS (MALDI): calculated: 710.63, found: 710.0 (M^+).

PDPP2TPCL. To a degassed solution of the monomer **M1** (41.90 mg, 0.061 mmol), **M2** (67.45 mg, 0.061 mmol) in toluene (2 mL) and DMF (0.2 mL) tris(dibenzylideneacetene)dipalladium(0) (1.69 mg, 1.83 μmol) and triphenylphosphine (1.93 mg, 7.32 μmol) were added. The mixture was stirred at 115 °C for 16 h, after which it was precipitated in methanol and filter through a Soxhlet thimble. The polymer was extracted with acetone, hexane, dichloromethane and then dissolved in 1,1,2,2-tetrachloroethane (TCE) (80 mL) at 140 °C, which was then precipitated into acetone. Finally the resulting polymer can be solubilized in $CHCl_3$ and toluene for device fabrication. Yield: 71.60 mg (90%). GPC (*o*-DCB, 140 °C): $M_n = 53.0$ kg mol^{-1}, $M_w = 109.5$ kg mol^{-1} and $Đ_M = 2.07$.

PMDPP2TPCL. Same procedure as for **PDPP2TPCL** was used, but now **M3** (53.59 mg, 0.077 mmol) and **M2** (84.53 mg, 0.077 mol) were used as the monomers. Yield: 89.00 mg (89%) as a dark solid. GPC (*o*-DCB, 140 °C): $M_n = 33.2$ kg mol^{-1}, $M_w = 72.0$ kg mol^{-1} and $Đ_M = 2.17$.

P2MDPP2TPCL. Same procedure as for **PDPP2TPCL** was used, but now **M4** (51.48 mg, 0.072 mmol) and **M2** (79.59 mg, 0.072 mol) were used as the monomers. Yield: 91.2 mg (94%) as a dark solid. GPC (*o*-DCB, 140 °C): $M_n = 20.4$ kg mol^{-1}, $M_w = 35.2$ kg mol^{-1} and $Đ_M = 1.73$.

Results and discussion

Synthesis

The synthetic procedures for the monomers and polymers are presented in Scheme 1. The starting compound **2** and **3** can be efficiently achieved by using the traditional method as shown in Scheme S1.† The monomer bisstannyl-PCL (**M1**),[30] the dibromo-monomer **M3** (ref. 26) and **M4** (ref. 25) were synthesized by using the similar procedures as reported in the literatures. The polymers **PDPP2TPCL**, **PMDPP2TPCL** and **P2MDPP2TPCL** were prepared *via* Stille polymerization, in which a $Pd_2(dba)_3/PPh_3$ (1 : 4) catalyst and toluene/DMF (10 : 1) solvent mixture were applied to achieve high molecular weight. The molecular weight of the polymers was determined by gel permeation chromatography (GPC) with *o*-DCB as eluent at 140 °C, as summarized in Table 1. The polymer **PDPP2TPCL** shows a number-average molecular weight (M_n) of 53.9 kg mol^{-1} and molar-mass dispersity ($Đ_M$)[31] of 2.0. In comparison, the methylated polymers **PMDPP2TPCL** and **P2MDPP2TPCL** exhibit relatively low M_n of 33.2 kg mol^{-1} and 20.4 kg mol^{-1}. It is worth mentioning that the polymer **PDPP2TPCL** was previously prepared *via* Suzuki polymerization and provided a high M_n of 72.8 kg mol^{-1} and $Đ_M$ of 3.3.[13] We also tried to prepare the methylated polymers *via* Suzuki reaction, but the synthesis of diboronic ester of methylated DPP monomers was failed.

Absorption spectra and energy levels

Absorption spectra of the polymers in chloroform solution and thin films were shown in Fig. 2 and the data was summarized at Table 1. All the three polymers have red-shift absorption spectra in thin films compared to that in solution. **PDPP2TPCL** has the optical band gap (E_g) of 1.44 eV with absorption onset at 864 nm in thin films, which is similar to that of the polymer prepared by Suzuki polymerization.[13] The methylated polymers **PMDPP2TPCL** and **P2MDPP2TPCL** show slightly high E_g of 1.47 eV and 1.50 eV, which may cause by the slightly steric hindrance between MT and PCL units.

The energy levels of the polymers were determined by cyclic voltammetry measurements, as shown in Fig. 2b and Table 1. **PDPP2TPCL** has HOMO and LUMO levels of −5.35 eV and −3.91 eV, while **PMDPP2TPCL** and **P2MDPP2TPCL** show slightly high-lying HOMO and LUMO levels of −5.30 eV (−5.24 eV) and −3.83 eV (−3.74 eV). Since the fullerene derivative, [70] PCBM has a LUMO level of −4.16 eV,[13] the LUMO offset between

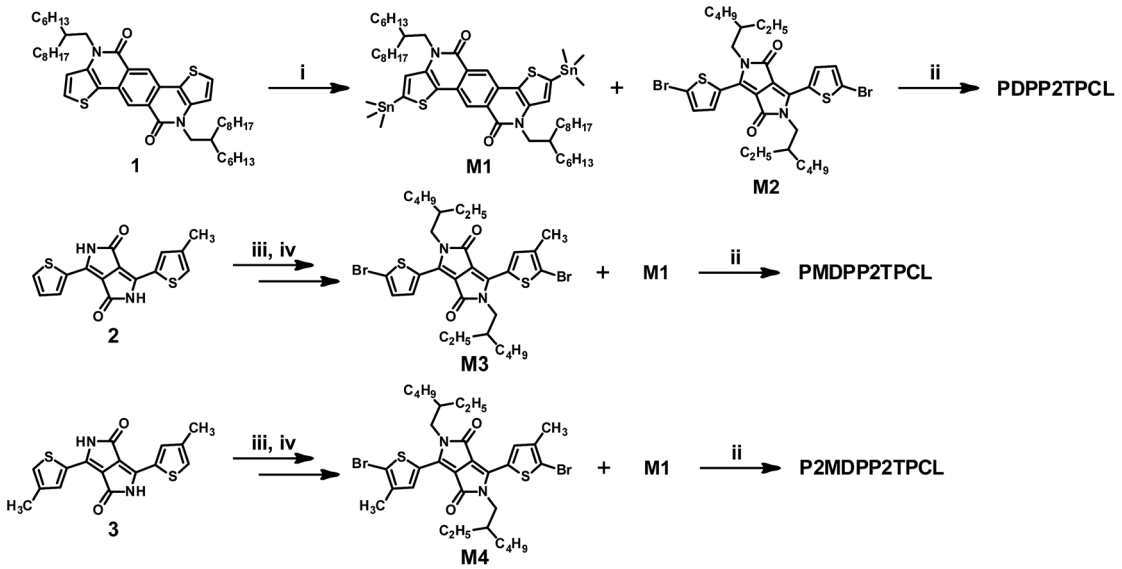

Scheme 1 Synthetic routes of the monomers and polymers. (i) LDA, −78 °C, and $Sn(CH_3)_3Cl$ at −78 °C. (ii) Stille polymerization by using $Pd_2(dba)_3/PPh_3$ in toluene/DMF (10 : 1, v/v) at 115 °C. (iii) K_2CO_3, 18-crown-6, and 2-ethylhexyl bromide in DMF at 120 °C, 16 h. (iv) Br_2 in $CHCl_3$.

Table 1 Molecular weight, optical, and electrochemical properties of the DPP polymers

			Solution			Film				
Polymer	M_n[a] (kg mol^{-1})	$Đ_M$	λ_{peak} (nm)	λ_{onset} (nm)	E_g (eV)	λ_{peak} (nm)	λ_{onset} (nm)	E_g (eV)	E_{HOMO}[b] (eV)	E_{LUMO}[c] (eV)
PDPP2TPCL	53.9	2.0	765	838	1.48	770	864	1.44	−5.35	−3.91
PMDPP2TPCL	33.2	2.2	757	816	1.52	763	846	1.47	−5.30	−3.83
P2MDPP2TPCL	20.4	1.7	750	809	1.53	756	826	1.50	−5.24	−3.74

[a] Determined with GPC at 140 °C using *o*-DCB as the eluent. [b] Determined using a work function value of −4.8 eV for Fc/Fc^+. [c] Determined as $E_{HOMO} + E_g^{film}$.

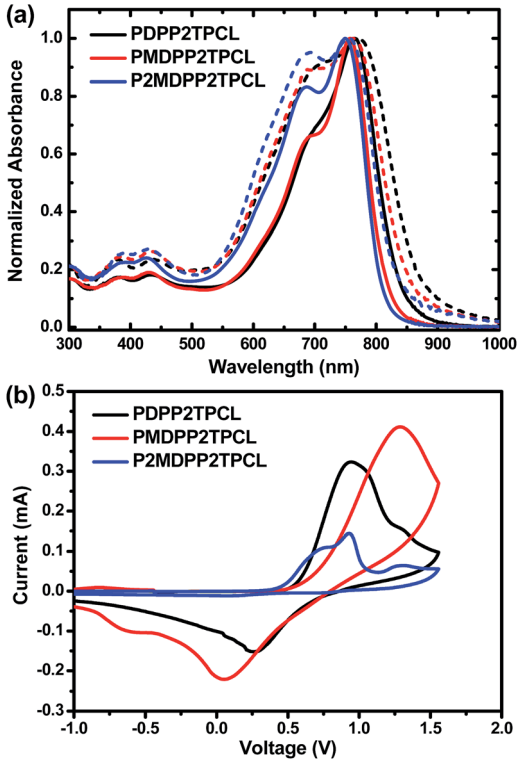

Fig. 2 (a) Absorption spectra (solid lines, in $CHCl_3$ solution; dash lines, in thin films) and (b) cyclic voltammograms of the DPP polymers. Potential *vs.* Fc/Fc^+.

the polymers and PCBM is increased from 0.25 eV for **PDPP2TPCL** to 0.42 eV for **P2MDPP2TPCL**. The enhanced energy offset will be helpful for exciton dissociation into free charges in solar cells.

Charge transport properties

The charge transport properties of the polymers are determined using field-effect transistor devices with a bottom gate–bottom contact (BGBC) configuration. The polymer thin films were deposited *via* spin coating from $CHCl_3$/*o*-DCB (10%) solution and thermally annealed for 10 min. The transfer and output curves are shown in Fig. 3, and the key parameters are summarized in Table 2. The polymer **PDPP2TPCL** exhibits a hole mobility (μ_h) of 0.56 $cm^2\ V^{-1}\ s^{-1}$ with a low threshold voltage (V_T) at −1.5 eV and a on/off ratio of 10^4, while the mobilities of **PMDPP2TPCL** and **P2MDPP2TPCL** are 0.57 and 0.47 $cm^2\ V^{-1}\ s^{-1}$, respectively. The three polymers exhibit very similar hole mobilities in FETs. These acceptor–acceptor polymers were also found to perform electron mobilities around 10^{-2} $cm^2\ V^{-1}\ s^{-1}$ in FETs (Fig. S1 and Table S1†). The ambipolar charge transports can also be found in other DPP polymers, such as alternating with the strong acceptor benzothiadiazole.[32,33]

We further use GIWAXS to study the morphology of the thin films, as shown in Fig. 4. **PDPP2TPCL** shows the strong (100) and (010) diffraction peaks in the out-of-plane direction, corresponding to the lamellar and π–π stacking of the polymers in thin films. This indicates that **PDPP2TPCL** has a mixed

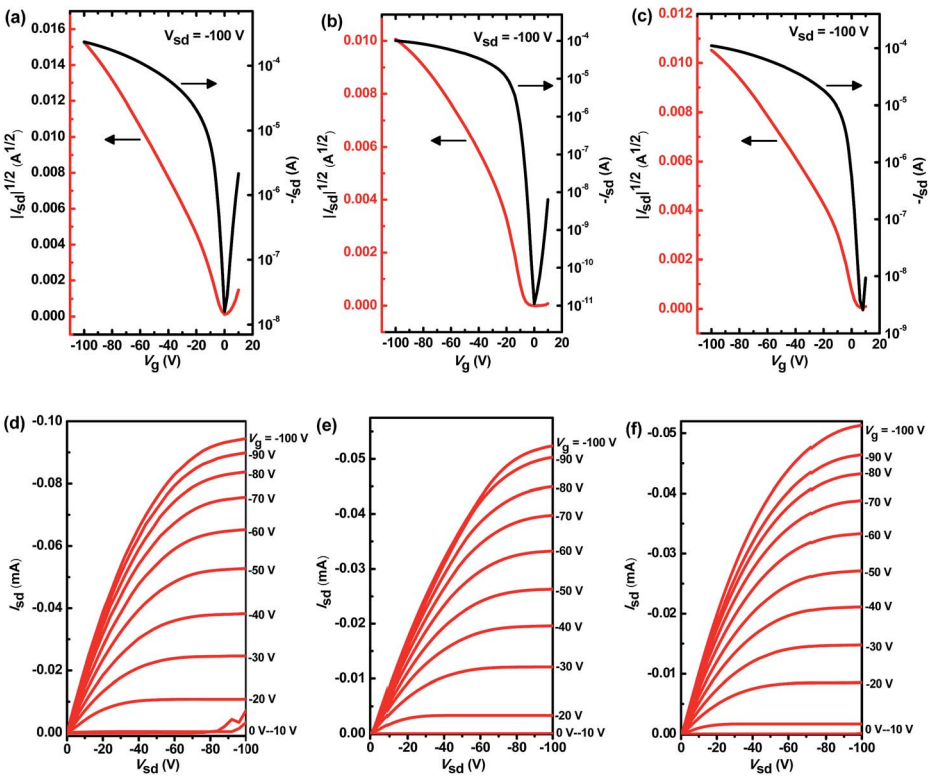

Fig. 3 (a–c) Transfer and (d–f) output curves obtained from BGBC FET devices for p-type characteristics. (a and d) for **DPP2TPCL**; (b and e) for **PMDPP2TPCL** and (c and f) for **P2MDPP2TPCL**. The thin films were spin cast from $CHCl_3$/*o*-DCB (10%) solution and annealed at 120 °C for **PDPP2TPCL** and **P2MDPP2TPCL**, and 150 °C for **PMDPP2TPCL**.

Table 2 Field-effect hole mobilities of the DPP polymers in a BGBC configuration. The parameters from GIWAXS were also included

Polymer	μ_h ($cm^2\ V^{-1}\ s^{-1}$)	V_T (V)	I_{on}/I_{off}	d (100) (nm)	d (010) (nm)
PDPP2TPCL	0.56	−1.5	1×10^4	1.95	0.37
PMDPP2TPCL	0.57	−7.2	9×10^6	1.94	0.36
P2MDPP2TPCL	0.47	2.9	4×10^4	1.94	0.37

orientation of "edge-on" and "face-on" orientation in thin films. The *d*-spacings of lamellar packing and π–π stacking are 1.95 nm and 0.37 nm (Table 2). **PMDPP2TPCL** with asymmetric structure also presents (100) and (010) diffraction peaks in the out-of-plane direction, but the (100) diffraction peak in the in-plane is also significantly increased. This means that **PMDPP2TPCL** has the tendency to form "face-on" orientation. **P2MDPP2TPCL** with MT as linkers present (100) diffraction peaks in the out-of-plane and in-plane direction, while the (010) diffraction peaks is significant reduced, corresponding to the reduced crystalline properties. The results indicate that although the introduction of methyl units into the polymers can reduce the crystalline properties, the hole mobility is still similar to that of non-methylated polymers.

Solar cells performance

The polymers as electron donor and [70]PCBM as electron acceptor were applied into solar cells by using the device configuration of ITO/PEDOT:PSS as cathode and LiF/Al as anode. The photo-active layers were spin coated from $CHCl_3$ solution, in which the fabrication condition including the additive, the ratio of donor to acceptor and the thickness of active layers was carefully optimized. In general, **PDPP2TPCL** and **P2MDPP2TPCL**:PCBM cells show the optimized performance when the ratio of donor to acceptor is 1 : 2 with the processing additive of DPE, while **PMDPP2TPCL**:PCBM shows the optimized cells with the ratio of donor to acceptor is 1 : 1.5.

The *J*–*V* characteristics and external quantum efficiency (EQE) of the optimized solar cells are shown in Fig. 5 and Table 3. The J_{sc}s were determined by integrating the EQE with the AM1.5G (100 mW cm^{-2}) spectrum.

PDPP2TPCL:PCBM cells show a PCE of 4.2% with J_{sc} of 8.3 mA cm^{-2}, V_{oc} of 0.76 V and FF of 0.66. The performance is slightly low compared to the cells based on **PDPP2TPCL** prepared from Suzuki polymerization.[13] **PMDPP2TPCL** based cells exhibit the best PCE of 6.1% with a high J_{sc} of 12.8 mA cm^{-2}, V_{oc} of 0.78 V and FF of 0.61. The polymer **P2MDPP2TPCL** provided a PCE of 6.0% with a J_{sc} of 13.3 mA cm^{-2} in solar cells. It is interesting to observe that methylated polymers have similar V_{oc} to that of non-methylated polymer, which is different from other methylated polymer solar cells with reduced V_{oc}.[25] The enhanced J_{sc}s of methylated polymer solar cells were also reflected by their external quantum efficiencies (EQEs), as present in Fig. 5b. **PDPP2TPCL**:PCBM cells show the broad photo-response from 300 nm to 850 nm with the maximum EQE of 0.27 in the polymer absorbed region, while the maximum

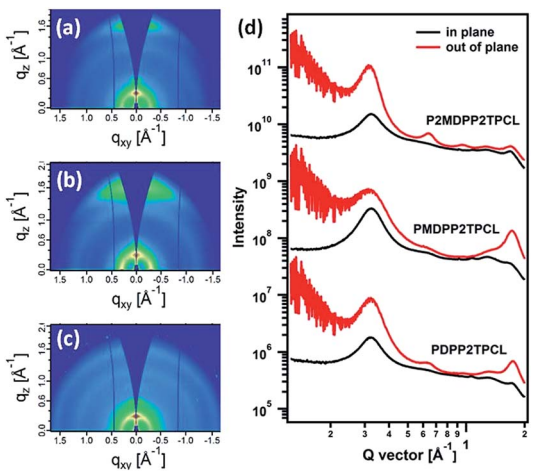

Fig. 4 GIWAXS images of (a) **PDPP2TPCL**, (b) **PMDPP2TPCL** and (c) **P2MDPP2TPCL** thin films. (d) The out-of-plane and in-plane cuts of the corresponding GIWAXS patterns. The fabrication condition for the pure thin films is summarized at Fig. 3.

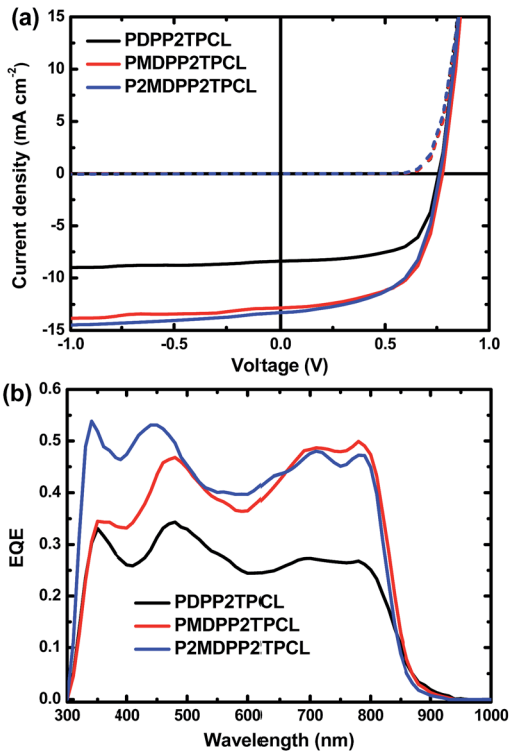

Fig. 5 (a) *J*–*V* characteristics in the dark (dashed lines) and under white light illumination (solid lines). (b) EQE of the optimized DPP polymer:[70]PCBM solar cells.

Table 3 Solar cell parameters of optimized solar cells of DPP polymers:$PC_{71}BM$

Polymer[a]	J_{sc}[b] (mA cm^{-2})	V_{oc} (V)	FF	PCE (%)	E_{loss} (eV)
PDPP2TPCL	8.3	0.76	0.66	4.2	0.68
PMDPP2TPCL	12.8	0.78	0.61	6.1	0.69
P2MDPP2TPCL	13.3	0.76	0.59	6.0	0.74

[a] Ratio of donor to acceptor is 1 : 1.5 for **PMDPP2TPCL** and 1 : 2 for **PDPP2TPCL** and **P2MDPP2TPCL**. Optimized spin coating solvent for active layer is $CHCl_3$ with 5% DPE as additive for the three polymers. [b] J_{sc} as calculated by integrating the EQE spectrum with the AM1.5G spectrum. The thickness of active layers is 120 nm for **PDPP2TPCL**, 110 nm for **PMDPP2TPCL** and 90 nm for **P2MDPP2TPCL**.

EQE was enhanced to 0.50 and 0.47 for **PMDPP2TPCL** and **P2MDPP2TPCL** based cells. The solar cells based these polymers also show the E_{loss} of 0.68–0.74 eV (Table 3), indicating the similar efficiency of exciton dissociation into free charges. Therefore, we propose that other reasons such as micro-phase separation in blended thin films may be responsible for the high photocurrent in methylated polymer solar cells.

Morphology investigation

Therefore, we intend to study the micro-phase separation of the blended thin films in detail. The morphology of the thin films was firstly investigated by AFM and TEM images, as shown in Fig. 6. From AFM images, we can observe the reduced roughness of the blended thin films, from 4 nm for **PDPP2TPCL**:PCBM to 3 nm and 2 nm for **PMDPP2TPCL** and **P2MDPP2TPCL** based thin films. This may indicate the more mixed blend based on methylated polymers. The observation can be further confirmed by TEM images, as shown in Fig. 6d–f. **PDPP2TPCL**:PCBM system shows clearly fibrillar structures with a large diameter (>20 nm), while **PMDPP2TPCL** and **P2MDPP2TPCL** based thin films have fine morphology with unclear fiber structures, indicating mixed thin films. This can also explain the reduced FF in solar cells based on methylated polymers.

We further use GIWAXS and R-SoXS to study the morphology of blended thin films based on these polymers, as shown in Fig. 7 and 8. We observe similar crystalline packing of the polymers in thin films in GIWAXS measurement, with strong (100) diffraction peaks in the out-of-plane and in-plane direction. The (010) diffraction peaks that are correlating to π–π stacking of the conjugated backbone are reduced, indicating that PCBM can disturb the crystal structure of the polymers. The *d*-spacings of lamellar and π–π stacking of the polymers in blended thin films are very similar to those of pure polymers (Table 4). We can calculate the coherence length (CL), in which the reduced CL for methylated polymers can be observed, correlating to the small crystal domain in methylated polymers based thin films.

The phase separation of the blended thin films is further investigated by the contrast enhanced technique R-SoXS, which is based on enhanced contrast between different organic components and provides information regarding the characteristic mode length (domain size) and average compositional fluctuation (domain purity). Fig. 8 shows the scattering profile of the blends at 284.2 eV. The scattering intensity of blended

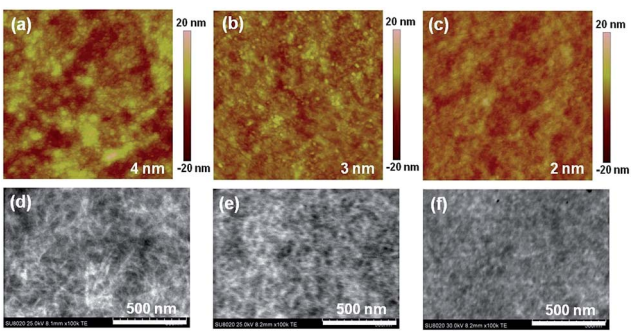

Fig. 6 (a–c) AFM height images (3 × 3 μm^2) and (d–f) TEM images of optimized DPP polymer:[70]PCBM thin films. The RMS roughness is included in the AFM images.

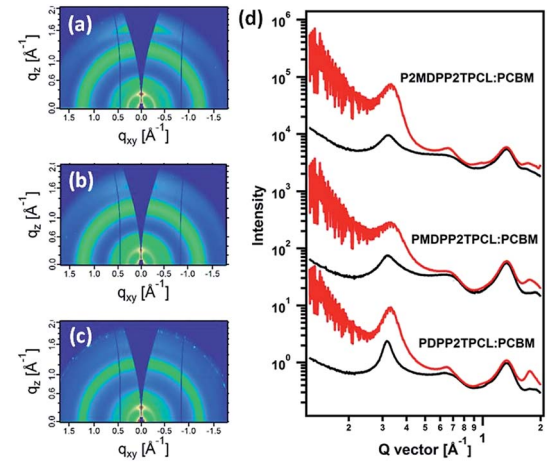

Fig. 7 GIWAXS images of (a) **PDPP2TPCL**, (b) **PMDPP2TPCL** and (c) **P2MDPP2TPCL** blended with PCBM thin films. (d) The out-of-plane and in-plane cuts of the corresponding GIWAXS patterns. The fabrication condition for the blended thin films was summarized at Table 3.

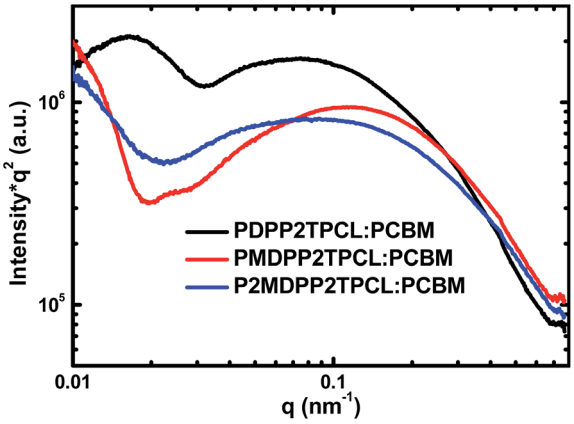

Fig. 8 R-SoXS scattering profiles at 284.2 eV of the polymers blended with PCBM.

Table 4 Crystallographic parameters of the blend thin films. OOP: out-of-plane. IP: in-plane. CL: coherence length

	IP (100)		OOP (010)			
	d-spacing [nm]	CL [nm]	*d*-spacing [nm]	CL [nm]	Domain size (nm)	Domain purity
PDPP2TPCL:PCBM	1.97	17.2	0.36	3.5	42	1
PMDPP2TPCL:PCBM	1.96	11.2	0.36	2.4	27	0.88
P2MDPP2TPCL:PCBM	1.95	9.8	0.37	—	36	0.82

thin films is normalized by the materials optical contrast. The domain size of 42 nm was found for **PDPP2TPCL**:PCBM thin film, which was decreased to 27 nm and 36 nm for methylated polymers based thin films (Table 4). The relative domain purity can be determined by integrating the profiles over q. The higher the total scattering intensity is, the purer the domains are. **PDPP2TPCL**:PCBM thin film exhibits higher domain purity compared to methylated polymer blended thin films (Table 4).

Morphology investigation by AFM, TEM, GIWAXS and R-SoXS reveals that methylated polymers have small domain size and finely micro-phase separation with PCBM, which is helpful for exciton diffusion into the interface of donor and acceptor. This can explain the high photocurrent in methylated polymer solar cells.

Conclusions

In conclusion, three conjugated polymers incorporating electron-deficient PCL and DPP units were designed for application in PSCs. The polymers contain different aromatic linkers, from thiophene to methylthiophene. Methylated polymers were found to show slightly blue-shift absorption and high-lying energy levels compared to the non-methylated polymers. The three polymers perform similar hole mobility of 0.47–0.57 cm^2 V^{-1} s^{-1}. Methylated polymers show a high PCE of 6.1% with a high J_{sc} of 12.8 mA cm^{-2} in solar cells, while the non-methylated polymer show a low PCE of 4.2% with a low J_{sc} of 8.3 mA cm^{-2}. The enhanced photocurrent in methylated polymer solar cells was attributed to the small crystal domain of the polymers in blended thin films, which is helpful for exciton diffusion into the interface of donor to acceptor. Our results demonstrate that conjugated polymers containing several electron-deficient units can realize high performance solar cells after intentional modification of chemical structures.

Acknowledgements

We thank Qiang Wang and Ralf Bovee at Eindhoven University of Technology for GPC analysis. This work was supported by the Recruitment Program of Global Youth Experts of China. The work was further supported by the National Natural Science Foundation of China (21574138, 91233205) and the Strategic Priority Research Program (XDB12030200) of the Chinese Academy of Sciences. W. M. thanks for the support from NSFC (21504006, 21534003, 51320105014). X-ray data was acquired at beamlines 7.3.3 and 11.0.1.2 at the Advanced Light Source, which is supported by the Director, Office of Science, Office of Basic Energy Sciences, of the U.S. Department of Energy under Contract No. DE-AC02-05CH11231.

Notes and references

1 J. Zhao, Y. Li, G. Yang, K. Jiang, H. Lin, H. Ade, W. Ma and H. Yan, *Nat. Energy*, 2016, **1**, 15021–15027.
2 W. Zhao, D. Qian, S. Zhang, S. Li, O. Inganäs, F. Gao and J. Hou, *Adv. Mater.*, 2016, **28**, 4734–4739.
3 F. C. Krebs, N. Espinosa, M. Hösel, R. R. Søndergaard and M. Jørgensen, *Adv. Mater.*, 2014, **26**, 29–39.
4 Y. J. Cheng, S. H. Yang and C. S. Hsu, *Chem. Rev.*, 2009, **109**, 5868–5923.
5 L. Lu, T. Zheng, Q. Wu, A. M. Schneider, D. Zhao and L. Yu, *Chem. Rev.*, 2015, **115**, 12666–12731.
6 D. Veldman, S. C. J. Meskers and R. A. J. Janssen, *Adv. Funct. Mater.*, 2009, **19**, 1939–1948.
7 W. Li, K. H. Hendriks, A. Furlan, M. M. Wienk and R. A. J. Janssen, *J. Am. Chem. Soc.*, 2015, **137**, 2231–2234.
8 K. Gao, L. Li, T. Lai, L. Xiao, Y. Huang, F. Huang, J. Peng, Y. Cao, F. Liu, T. P. Russell, R. A. J. Janssen and X. Peng, *J. Am. Chem. Soc.*, 2015, **137**, 7282–7285.
9 N. A. Ran, J. A. Love, C. J. Takacs, A. Sadhanala, J. K. Beavers, S. D. Collins, Y. Huang, M. Wang, R. H. Friend, G. C. Bazan and T.-Q. Nguyen, *Adv. Mater.*, 2015, **28**, 1482–1488.
10 K. Kawashima, Y. Tamai, H. Ohkita, I. Osaka and K. Takimiya, *Nat. Commun.*, 2015, **6**, 10085.
11 Y. Li, X. Liu, F.-P. Wu, Y. Zhou, Z.-Q. Jiang, B. Song, Y. Xia, Z.-G. Zhang, F. Gao, O. Inganas, Y. Li and L.-S. Liao, *J. Mater. Chem. A*, 2016, **4**, 5890–5897.
12 J. Liu, S. Chen, D. Qian, B. Gautam, G. Yang, J. Zhao, J. Bergqvist, F. Zhang, W. Ma, H. Ade, O. Inganäs, K. Gundogdu, F. Gao and H. Yan, *Nat. Energy*, 2016, **1**, 16089.
13 G. Feng, Y. Xu, C. Xiao, J. Zhang, X. Zhang, C. Li, Z. Wei, W. Hu, Z. Wang and W. Li, *Polym. Chem.*, 2016, **7**, 164–170.
14 R. S. Ashraf, A. J. Kronemeijer, D. I. James, H. Sirringhaus and I. McCulloch, *Chem. Commun.*, 2012, **48**, 3939–3941.
15 J.-K. Lee, M. C. Gwinner, R. Berger, C. Newby, R. Zentel, R. H. Friend, H. Sirringhaus and C. K. Ober, *J. Am. Chem. Soc.*, 2011, **133**, 9949–9951.
16 G. Kim, A. R. Han, H. R. Lee, J. Lee, J. H. Oh and C. Yang, *Chem. Commun.*, 2014, **50**, 2180–2183.
17 C.-W. Ge, C.-Y. Mei, J. Ling, J.-T. Wang, F.-G. Zhao, L. Liang, H.-J. Li, Y.-S. Xie and W.-S. Li, *J. Polym. Sci., Part A: Polym. Chem.*, 2014, **52**, 1200–1215.

18 F. Grenier, P. Berrouard, J.-R. Pouliot, H.-R. Tseng, A. J. Heeger and M. Leclerc, *Polym. Chem.*, 2013, **4**, 1836–1841.
19 P. Wang, H. Li, C. Gu, H. Dong, Z. Xu and H. Fu, *RSC Adv.*, 2015, **5**, 19520–19527.
20 Y. Ji, C. Xiao, G. H. L. Heintges, Y. Wu, R. A. J. Janssen, D. Zhang, W. Hu, Z. Wang and W. Li, *J. Polym. Sci., Part A: Polym. Chem.*, 2016, **54**, 34–38.
21 K. Mahmood, H. Lu, Z.-P. Liu, C. Li, Z. Lu, X. Liu, T. Fang, Q. Peng, G. Li, L. Li and Z. Bo, *Polym. Chem.*, 2014, **5**, 5037–5045.
22 W. Li, K. H. Hendriks, M. M. Wienk and R. A. J. Janssen, *Acc. Chem. Res.*, 2016, **49**, 78–85.
23 C. B. Nielsen, M. Turbiez and I. McCulloch, *Adv. Mater.*, 2013, **25**, 1859–1880.
24 S. Y. Qu and H. Tian, *Chem. Commun.*, 2012, **48**, 3039–3051.
25 W. Li, A. Furlan, K. H. Hendriks, M. M. Wienk and R. A. J. Janssen, *J. Am. Chem. Soc.*, 2013, **135**, 5529–5532.
26 Y. Ji, C. Xiao, Q. Wang, J. Zhang, C. Li, Y. Wu, Z. Wei, X. Zhan, W. Hu, Z. Wang, R. A. J. Janssen and W. Li, *Adv. Mater.*, 2016, **28**, 943–950.
27 E. Zhou, S. Yamakawa, K. Tajima, C. Yang and K. Hashimoto, *Chem. Mater.*, 2009, **21**, 4055–4061.
28 H. Alexander, B. Wim, G. James, S. Eric, G. Eliot, K. Rick, M. Alastair, C. Matthew, R. Bruce and P. Howard, *J. Phys.: Conf. Ser.*, 2010, **247**, 012007.
29 E. Gann, A. T. Young, B. A. Collins, H. Yan, J. Nasiatka, H. A. Padmore, H. Ade, A. Hexemer and C. Wang, *Rev. Sci. Instrum.*, 2012, **83**, 045110.
30 I. H. Jung, W.-Y. Lo, J. Jang, W. Chen, D. Zhao, E. S. Landry, L. Lu, D. V. Talapin and L. Yu, *Chem. Mater.*, 2014, **26**, 3450–3459.
31 R. F. T. Stepto, *Polym. Int.*, 2010, **59**, 23–24.
32 P. Sonar, S. P. Singh, Y. Li, M. S. Soh and A. Dodabalapur, *Adv. Mater.*, 2010, **22**, 5409–5413.
33 S. Cho, J. Lee, M. H. Tong, J. H. Seo and C. Yang, *Adv. Funct. Mater.*, 2011, **21**, 1910–1916.